

Article

Designing Self Supported SLM Structures via Topology Optimization

B. Barroqueiro ^{1,2,*} , A. Andrade-Campos ¹  and R. A. F. Valente ¹

¹ Department of Mechanical Engineering, Centre for Mechanical Technology & Automation, University of Aveiro, 3810-193 Aveiro, Portugal

² Active Space Technologies, Actividades Aeroespaciais S.A., Parque Industrial de Taveiro, Lote 12, 3045-508 Coimbra, Portugal

* Correspondence: bjfb@ua.pt

Received: 27 June 2019; Accepted: 6 August 2019; Published: 8 August 2019



Abstract: The potential of Additive Manufacturing (AM) is high, with a whole new set of manufactured parts with unseen complexity being offered. However, the process has limitations, and for the sake of economic competitiveness, these should also be considered. Therefore, a computational methodology, capable of including the referenced limitations and providing initial solid designs for Selective Laser Melting (SLM) is the subject of the present work. The combination of Topology Optimization (TO) with the simplified fabrication model is the selected methodology. Its formulation, implementation, and integration on the classic TO algorithm is briefly discussed, being capable of addressing the minimum feature size and the overhang constraint limitations. Moreover, the performance and numerical stability of the methodology is evaluated, and numerical variables, such as the accuracy of structural equilibrium equations and the material interpolation model, are considered. A comparative study between these variables is presented. The paper then proposes an enhanced version of the selected methodology, with a better convergence towards a discrete solution.

Keywords: AM limitations; topology optimization; overhang constraints

1. Introduction

Metal Additive Manufacturing (AM), in particular Selective Laser Melting (SLM) and Electron Beam Melting (EBM), is at the forefront of the advanced manufacturing technologies [1]. These consist of the manufacturing of the 3D model layer by layer, allowing a great design freedom. On the other hand, Topology Optimization (TO) is a type of structural optimization that seeks the optimum material layout [2] and thus provides the means for intelligently exploring this freedom. In this way, the interconnection between AM and TO has proven to be advantageous [3]. Moreover, Figure 1 illustrates their interplay, as well as their main steps and key advantages.

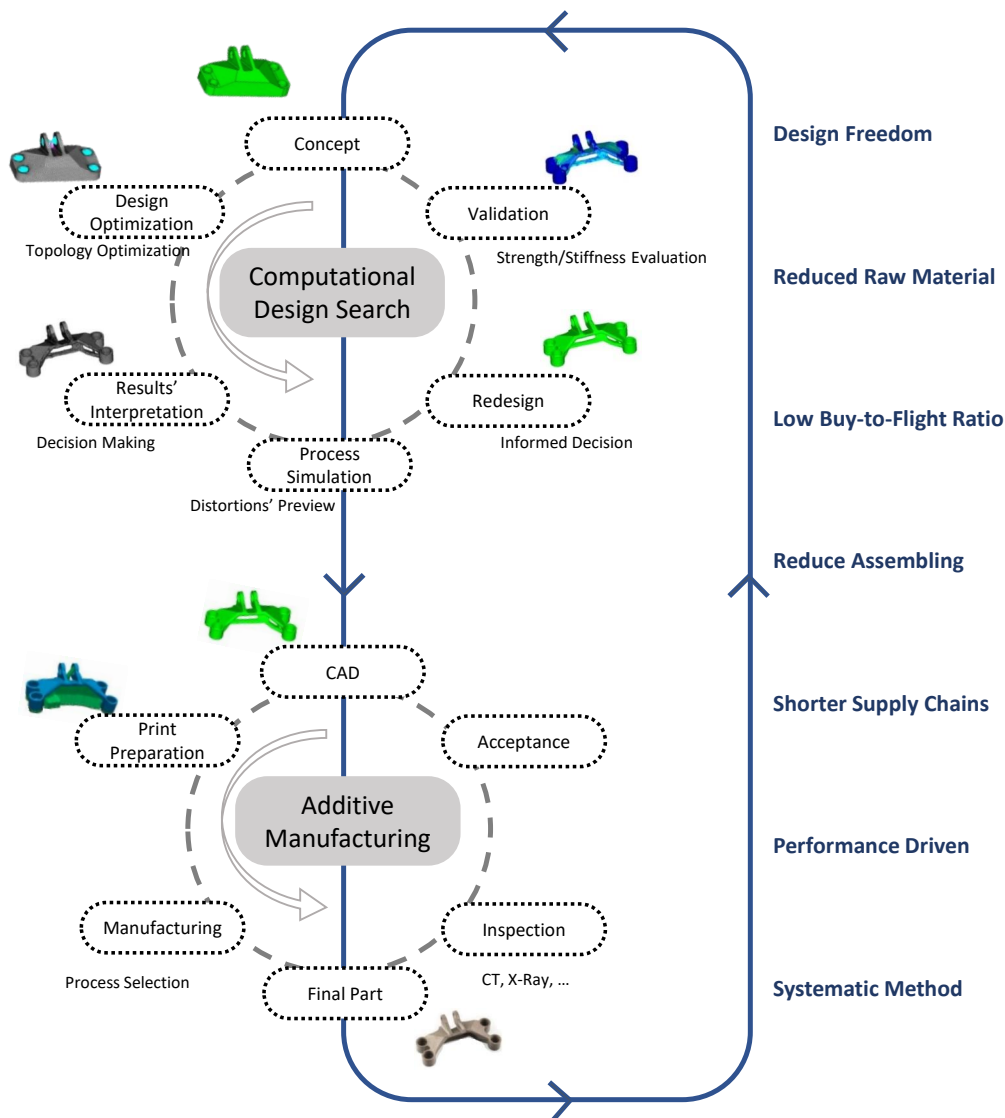


Figure 1. The interplay between additive manufacturing and topology optimization (bracket's figures extracted from Komi [4]).

The current market trends indicate that clients are increasingly demanding mass customization instead of mass production, and therefore, industry needs to adapt in order to be successful. Therefore, effective and flexible processes are needed in order to reduce the time to market and the development cycles [5]. Moreover, engineers and designers are encouraged to reduce geometric complexity, since there is a direct link between costs and part complexity. Within this context, Additive Manufacturing (AM) is seen as a disruptive technology [6,7] with the potential to overcome a number of limitations of traditional processes. These advantages can be grouped into:

- shape complexity: it is possible to take advantage of great geometrical freedom in order to reduce several parts in an assembly and/or using design optimization methodologies (TO), which opens a new world of customization possibilities [8–10];
- material complexity: multi-material parts can be built [11–13]; non-weldable materials can be joined [14]; coatings can be applied [15,16]; and surface finishing can be performed (polishing) [17];
- hierarchical complexity: multi-scale structures can be designed and fabricated using a geometric mesostructure in order to provide information to the part-scale macrostructure (i.e., lattices with negative or zero or positive coefficients of thermal expansion) [9,18,19];

- operational simplicity: AM allows for simpler supply chains and, therefore, shorter lead-times, lower inventories (less expensive storage), and no tooling (i.e., molds) [9,10,20].

According to Nickels [21], the aerospace industry can greatly benefit from AM technologies, with several advantageous applications being reported. For instance, the development time frame of a component (i.e., structural brackets) can be reduced from six months to just one using AM technologies, since the part is produced directly from 3D without tooling. Another driver for the aerospace industry is the highly-expensive storage of rarely-used spare parts all around the world. Due to its operational simplicity, the alternative is using the AM technology to produce the spare parts on site and just in time.

However, the unclear part is its limitations as reported by Weller et al. [10] and Kelly [22]; there are several AM limitations, namely: build size, reproducibility, surface finishing, low build rate, skilled and experienced labor, standardization, and lack of design tools and guidelines to exploit the technology fully. Thus, the article's goal is a computational methodology capable of providing initial solid designs for metal AM, in particular SLM. Moreover, process limitations can also be accounted for in the referenced methodology. Therefore, the study presents its limitations in a succinct manner, as well as the main methodologies to overcome the referenced limitations. In this way, the rationale behind the present methodology is available, as well as the other alternatives, each one with its advantages and disadvantages. Then, the paper presents the selected methodology in a succinct manner, which is based on the TO filter and fabrication model in order to impose a minimum member size and an overhang constraint, respectively. The methodology presentation includes a succinct problem formulation, the computational algorithm structure and implementation, the performance evaluation, and an industrial application. Regarding performance evaluation, two well-known problems are considered: cantilever and MBB. During the TO of the referenced problems, variables such as: (i) the material interpolation model, (ii) the precision of structural equilibrium (approximated structural equilibrium versus a full precision industry solver), and (iii) the existence of a simplified fabrication model are considered in order to evaluate their impact in the convergence of TO, as well as their industrial applicability. After this study, an improved version of the simplified fabrication model is presented, showing a greater ability to converge to discrete solutions.

2. Current State of AM Limitations and Its Design Approaches

Powder bed fusion processes, in particular SLM, provide a cost-effective and time-efficient way of producing highly-customized low-volume parts [23]. While AM seems to have unlimited potential, it does not have unlimited applicability [24]. In fact, the design stage shall be meticulously carried out in order to take full advantage of AM. Thus, Design for Additive Manufacturing (DfAM) is an important research topic. Studies such as Thomas [25], Vayre et al. [26,27], Adam and Zimmer [28], Klahn et al. [29], Kranz et al. [30], Lemu and Gebisa [31], and Sossou et al. [32] focused on stabilizing design rules for AM, which are crucial for achieving competitive and successful parts.

The current limitations of the AM processes can be grouped into non-directional and directional constraints. Non-directional constraints are the minimum feature size and cavities, while directional constraints can be seen as warping, anisotropy, and overhangs [3]. In a nutshell, these are:

- The minimum feature size is important in order to guarantee the manufacturability: for instance, the SLM processes cannot print walls with less than 0.4 mm [25];
- Regarding cavities, the design shall ensure that all cavities have exit points for the non-melted powder. For simple cavities, one exit can be sufficient, but more complex geometries require more than one exit point. On the other hand, the use of these cavities can avoid issues such as material accumulation or a large volume of solid material [30];
- Regarding warping, its occurrence is related to the local melting and non-uniform cooling, which causes the referenced effect. Strains such as thermal, creep, and phase transformations are the causes of residual stresses [14]. In order to avoid warping, support structures can be used [3];

- Regarding anisotropy, AM can create parts that often exhibit anisotropy between the in-plane and out-of-plane directions. This issue is a direct consequence of the layer-wise construction, but the origin of this phenomenon is related to the resultant microstructures, being explained in detail in DebRoy et al. [14].
- Concerning the overhang constraints, their construction at zero degrees is not advisable, since the molten pool would simply sink into the powder. Even, if a support structure is used, the resultant geometry will be inaccurate with poor surface quality [25]. Thus, this constraint shall be considered. The solution can either be the use of chamfers and/or optimizing the build direction in order to maximize the overhang angles. A 45° angle is usually indicated as an acceptable threshold [25].

The intelligent search for a design that seeks the optimal material distribution (i.e., minimum compliance) and accounts for the previous constraints poses a greater challenge. Studies such as Joshi and Sheikh [33], Reddy K. et al. [34], Mirzendehtel and Suresh [35], Walton and Moztarzadeh [36], Allaire et al. [37], and Guo et al. [38] indicated that TO may provide the answer. Moreover, this method can include in its formulation some of the previous constraints and, thus, provide a solid initial design. The inclusion of AM constraints in the formulation of the TO algorithm has received some attention from the scientific community, namely the overhang constraints. In TO algorithms, the minimum feature size can be controlled by the radius of the filtering operation [3]. These are largely studied and reviewed in works such as Sigmund [39], Svanberg and Svärd [40], where extensive studies on the existing filters are available. On the other hand, imposing the overhang constraints on the topology optimization poses a greater problem, due to the implicit high non-linearity. Currently, there are several approaches to tackle the overhang constraint. These are:

- Modifying the design in order to limit the overhang to a certain limit. Since this approach is a post-processing technique, the resulting geometries have their ratio mass and stiffness compromised. For further details, consult Leary et al. [41];
- Using two scale calculations: a discrete scale where the overhang constraints are enforced and a continuous scale that uses the information from the discrete scale in order to produce self-supporting structures [42]. Alternative to the use of two macroscales (discrete and continuous) is the use of a mesoscale and a macroscale, where the mesoscale is defined by a Representative Unit Cell (RUC) and the macroscale uses the information of the homogenized mesoscale [43–45]. Thus, the RUC can be chosen to be self-supporting, but some manufacturing restrictions arise, namely minimum dimensions and extraction of non-melted powder;
- Using local constraints, being a simple and effective implementation. However, local constraints are expensive to compute and not very well suited for large-scale problems [46];
- Using edge detection algorithms to control the overhang angles [47–49]. The suppression method of intermediate densities in Qian [47] and Mezzadri et al. [49] uses an additional constraint, while the work in Garaigordobil and Ansola [48] used a Heaviside projection;
- Using simplified fabrication models, which stand for a low computational cost operation. Moreover, this does not require additional constraints to the optimization problems. Currently, there are two main AM fabrication models, one based on min-max operators [50–52], the other being based on area occupation and Heaviside projections [53–56], which can provide self-supporting designs.

In short, the last approach is considered the way forward, due to its computational cost and its simple integration on existent TO codes. Their drawback is related to the impossibility of parallel computing since the simplified fabrication model imposes that the algorithm must proceed in a layer-wise manner. In a preliminary analysis, this limitation can be seen as prohibitive. However, after a deep analysis, the relevance of this limitation becomes rather limited, if the implementation is properly structured. Thus, these fabrication models can be subdivided into three main steps. The first step corresponds to the supporting region search, which is computationally expensive, but can be

fully parallelized. The second and third steps correspond to sensitivities and densities scanning in a layer-wise manner in order to impose the overhang constraint. These steps are not parallelizable. However, their computational cost is marginal when compared with the structural equilibrium required by TO. In the current implementation, the difference is several orders of magnitude. The simplified fabrication model based on Heaviside projections requires high Heaviside penalization, making it highly susceptible to local minima. Moreover, if low Heaviside penalization is used, the algorithm converges to the classic solutions and uses intermediate densities to support it, defeating its purpose. The model based on min-max operators [50,51], which has already gained commercial applicability [52], exhibits good convergence properties and is less susceptible to be trapped in local minima. Therefore, the authors defend a preference for the last referenced approach due to its numerical performance. Therefore, the next section presents the topology optimization algorithm in order to explain the integration fabrication model in the referenced algorithm.

3. Topology Optimization

3.1. Standard Algorithm

3.1.1. Problem Formulation

Topology Optimization (TO) is a type of structural optimization that seeks the optimum material layout [2]. There are numerous methods to perform TO with a compressive list being available in Rozvany and Lewiński [57] and Deaton et al. [58]. Within the present work, density methods were used, namely the well-known Solid Isotropic Material with Penalization (SIMP) [59,60] and the Rational Approximation of Material Properties (RAMP) [61]. Both approaches seek the optimal material distribution, \mathbf{x} , across the design domain, Ω , in order to minimize compliance (for example). Thus, the classic TO problem of compliance minimization of a quasi-static loaded structure can be mathematically formulated as:

$$\min f(\mathbf{x}) = \mathbf{U}^T \mathbf{K}(\mathbf{x}) \mathbf{U}, \tag{1}$$

subjected to:

$$\begin{aligned} \mathbf{K}(\mathbf{x}) \mathbf{U} &= \mathbf{F}, \\ \sum_{e \in \Omega} \frac{V_e \rho_e(\mathbf{x})}{V_\Omega} &= V_f, \quad e \in \Omega \quad \text{and} \\ 0 < \mathbf{x}_e &< 1, \end{aligned} \tag{2}$$

where \mathbf{U} , \mathbf{F} , and \mathbf{K} are the global displacements, forces, and stiffness matrices, respectively. Furthermore, \mathbf{x} represents the design densities, which become physical densities (ρ) after filtering. Additionally, V_f , V_e , and V_Ω stand for the volume fraction (constraint), the volume of the element, and the domain, respectively. Using the SIMP approach, the element stiffness matrix, \mathbf{K}_e , becomes:

$$\mathbf{K}_e = \left(\rho_{\min} + \rho_e^\eta \right) \mathbf{K}_e^0, \tag{3}$$

where \mathbf{K}_e^0 is the stiffness matrix of the solid element, ρ_{\min} is a small constant to avoid an ill-conditioned system of equations, and η is the penalty parameter. Alternatively, using RAMP, the element stiffness matrix, \mathbf{K}_e , becomes:

$$\mathbf{K}_e = \left(\rho_{\min} + \frac{\rho_e}{1 + \eta(1 - \rho_e)} \right) \mathbf{K}_e^0, \tag{4}$$

where \mathbf{K}_e^0 is the stiffness matrix of the solid element multiplied by $1/(1 + \rho_{\min})$ [55] and η is again the penalty parameter.

3.1.2. Minimum Member Size

In order to ensure the existence of a solution, to impose a minimum member size and avoid problems such as the formation of checkerboard patterns, a filtering operation is recommended. The linear density filter (e.g., Bruns and Tortorelli [62], Bourdin [63]) can be formulated as:

$$\rho_e = \sum_{k \in N} w_{ek} \mathbf{x}_k, \tag{5}$$

where N defines the filtering neighborhood, composed by a set of elements, k [40]. Thus, $N_e = \{e : d(e, k) \leq r\}$, where $d(e, k)$ is the distance between the centroids of elements e and k . Considering conic weights, w_{ek} becomes:

$$w_{ek} = \begin{cases} \frac{r-d(e,k)}{\sum_{l \in N} r-d(e,l)} & , \quad k \in N_e \\ 0 & , \quad k \notin N_e. \end{cases} \tag{6}$$

Within the scope of this work, an extension of the density filter is used. Initially proposed by [64], this filter uses the Heaviside function, formulated as:

$$\rho_e = \frac{\tanh(\beta\varphi) + \tanh(\beta(\mu_e - \varphi))}{\tanh(\beta\varphi) + \tanh(\beta(1 - \varphi))} \quad \text{and} \tag{7}$$

$$\mu_e = \sum_{k \in N} w_{ek} \mathbf{x}_k, \tag{8}$$

where φ is set to 0.5. Additionally, β controls the “aggressiveness” of the Heaviside function [50].

3.1.3. Sensitivity Analysis

The derivatives of the objective function and constraint function for the independent variable, \mathbf{x} , are computed using the chain rule as:

$$\frac{\partial f}{\partial \mathbf{x}} = \frac{\partial f}{\partial \rho} \frac{\partial \rho}{\partial \mathbf{x}}. \tag{9}$$

Using SIMP, the first term is given by:

$$\frac{\partial f}{\partial \rho} = -\eta \rho_e^{\eta-1} \mathbf{u}_e^T \mathbf{k}_e^0 \mathbf{u}_e, \tag{10}$$

where \mathbf{u}_e and \mathbf{k}_e^0 are displacements and the stiffness matrix, respectively, associated with element e . Alternately, using RAMP, the first term is given by:

$$\frac{\partial f}{\partial \rho} = -\frac{\eta + 1}{(\eta(\rho_e - 1) - 1)^2} \mathbf{u}_e^T \mathbf{k}_e^0 \mathbf{u}_e. \tag{11}$$

Finally, the second term is computed using the chain rule as:

$$\frac{\partial \rho}{\partial \mathbf{x}} = \frac{\partial \rho}{\partial \mu} \frac{\partial \mu}{\partial \mathbf{x}} = \sum_{k \in N} w_{ek} \frac{\beta (\operatorname{sech}(\beta(\mu_k(\mathbf{x}) - \varphi))^2}{\tanh(\beta\varphi) + \tanh(\beta(1 - \varphi))}. \tag{12}$$

3.2. Simplified Fabrication Model

3.2.1. Integration in TO

This section briefly presents a methodology that allows the control of overhang angles (simplified fabrication model), as well as its integration in the classic topology optimization algorithm, being

based on min-max operators [50,51]. This algorithm proceeds in a layer-wise manner, mimicking the actual AM process. Thus, the algorithm starts on the first layer (that would be printed) up to the last layer. During this process, the densities of layer i cannot be higher than the maximum of the densities in the support region defined in layer $i - 1$. For the 2D case, the support region, $S(i, j)$, is defined according to Figure 2. It is worth noting that if a regular mesh (squares) is used, then an implicit overhang constraint of 45° is imposed, the extension to 3D being straightforward [51].

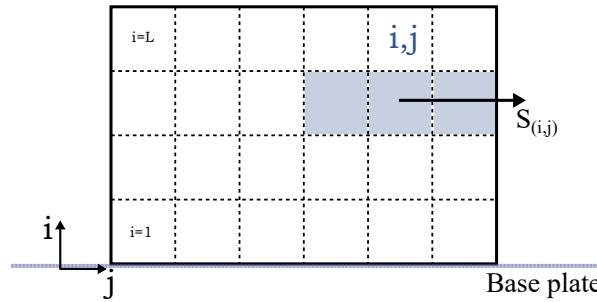


Figure 2. Definition of support region, $S(i, j)$, for the element (i, j) [50].

Thus, the smooth approximation of this constraint is formulated as:

$$\xi_{(i,j)} = \text{smin}(\rho_{(i,j)}, \Xi_{(i,j)}) = \frac{1}{2} \left(\rho_{(i,j)} + \Xi_{(i,j)} - \left((\rho_{(i,j)} - \Xi_{(i,j)})^2 + \epsilon \right)^{\frac{1}{2}} + \sqrt{\epsilon} \right), \quad (13)$$

$$\Xi_{(i,j)} = \text{smax} \left(\xi_{(i-1,j-1)}, \xi_{(i-1,j)}, \xi_{(i-1,j+1)} \right) = \left(\xi_{(i-1,j-1)}^P + \xi_{(i-1,j)}^P + \xi_{(i-1,j+1)}^P \right)^{\frac{1}{Q}} \quad (14)$$

$$\text{with } Q = P + \frac{\log(n_S)}{\log(\rho_0)}, \quad \xi_{(1,j)} = \rho_{(1,j)} \quad \text{and} \quad 1 < i \leq L, \quad (15)$$

where P , ρ_0 , and ϵ are constants, n_S is the size of the region S (meaning three in 2D), and L is the number of layers. The new density, ξ , is called the printed density. These densities result from the application of the previous equations to the physical densities. Since every ξ_i is dependent of all ξ_{i-1} , the calculation of the print densities shall proceed in a layer-wise manner, starting with the first layer up to the last. On the first layer, printed densities are equal to the physical densities. On the second layer, printed densities from the previous layer are used to compute *smax* (maximum density of region S), and then, *smin* is computed using the physical density of the current layer and the maximum from the previous layer (minimum between both). For the third layer and the remaining ones, the process is repeated.

Regarding the evaluation of the objective function, the printed densities are the ones that should be used, meaning that in Equation (3) or (4), the term ρ is replaced by ξ .

3.2.2. Sensitivity Analysis

The sensitivity analysis of the standard topology optimization requires some changes. The chain rule differentiation (Equation (9)) requires an additional term, becoming:

$$\frac{\partial f}{\partial \mathbf{x}} = \frac{\partial f}{\partial \xi} \frac{\partial \xi}{\partial \rho} \frac{\partial \rho}{\partial \mathbf{x}}. \quad (16)$$

the term $\partial f / \partial \xi$ corresponds to:

$$\frac{\partial f}{\partial \xi_e} = -\eta \xi_e^{\eta-1} \mathbf{u}_e^T \mathbf{k}_e^0 \mathbf{u}_e \quad \text{or} \quad (17)$$

$$\frac{\partial f}{\partial \xi_e} = -\frac{\eta + 1}{(\eta(\xi_e - 1) - 1)^2} \mathbf{u}_e^T \mathbf{k}_e^0 \mathbf{u}_e, \quad (18)$$

using SIMP or RAMP, respectively. The term $\partial \rho / \partial x$ is already defined by Equation (12). The term $\partial \xi / \partial \rho$ is the referenced additional term. This term is computed via an adjoint formulation (in addition to the adjoint formulation of TO), with its full formulation being shown in [50,51]. Briefly and given the sensitivities $\partial f / \partial \xi$, the present procedure modifies them in order to compute $\partial f / \partial \rho$. Thus, the procedure can be formulated as follows:

$$\frac{\partial f}{\partial \rho_i} = \lambda_i^T \frac{\partial smin_i}{\partial \rho_i} \quad \text{and} \tag{19}$$

$$\lambda_i^T = \begin{cases} \frac{\partial f}{\partial \xi_i} + \lambda_{i+1}^T \frac{\partial smin_{i+1}}{\partial \xi_i} & \text{for } 1 \leq i < L \\ \frac{\partial f}{\partial \xi_i} & \text{for } i = L \end{cases}, \tag{20}$$

where i stands for the layer index and $i + 1$ stands for the layer above, and therefore, each multiplier depends on the layer above. The algorithm modifies the existent sensitivities in the reversed print direction, meaning that the algorithm starts on the last layer until the first. The remaining derivatives are computed as:

$$\frac{\partial smin}{\partial \rho} = \frac{1}{2} \left(1 - (\rho_i - \Xi_i) \left((\rho_i - \Xi_i)^2 + \epsilon \right)^{-\frac{1}{2}} \right), \tag{21}$$

$$\frac{\partial smin}{\partial \xi} = \frac{\partial smin}{\partial \Xi} \frac{\partial \Xi}{\partial \xi}, \tag{22}$$

$$\frac{\partial smin}{\partial \Xi} = \frac{1}{2} \left(1 + (\rho_i - \Xi_i) \left((\rho_i - \Xi_i)^2 + \epsilon \right)^{-\frac{1}{2}} \right) \quad \text{and} \tag{23}$$

$$\frac{\partial \Xi_k}{\partial \xi_i} = \frac{P}{Q} \xi_i^{P-1} \left(\sum_{k \in S} \xi_k^P \right)^{\frac{1}{Q}}. \tag{24}$$

3.2.3. Modified Fabrication Model

Following the work of [50], the study points out that the *smax* operator has numerical problems. Initially, the study proposed the use of the P max function as the *smax* operator, but it suffered from severe overestimation, and then, the P-Q max function was proposed to tackle the referenced issue. However, the proposed solution solved the problem partially, since the operator can still accumulate relevant errors. Thus, this issue motivated the search for another smooth max function that would reduce the referenced errors. The function denominated as *softmax* [65] can be an interesting alternative, since this function does not produce overshoot. This function can be expressed as:

$$smax(\xi_i) = \Xi(\xi_i) = \frac{\sum_{i \in S} \xi_i e^{P \xi_i}}{\sum_{i \in S} e^{P \xi_i}}, \tag{25}$$

where $P > 0$, and its gradient is expressed as:

$$\frac{\partial \Xi_k}{\partial \xi_i} = \frac{e^{P \xi_i}}{\sum_{k \in S} e^{P \xi_k}} [1 + P (\xi_i - \Xi)]. \tag{26}$$

Thus, this function can be used as the new *smax* operator instead of the P-Q max function. In order to quantify the precision increase of the new *smax* operator, several support regions $(\xi_{(i-1,j-1)}, \xi_{(i-1,j)}, \xi_{(i-1,j+1)})$ were generated randomly, and their maximum was computed using the P-Q max and the *softmax* functions. Considering a “large number” of random support regions, the P-Q max function (for $P = 40$) provides a maximum absolute error (difference between real maximum and maximum smooth approximation) about 0.02, and around 7% of the support regions still get overestimated (these values may vary for different random number generators). The reader may

consider that an absolute error of 0.02 has limited relevance; however, it should be highlighted that this algorithm proceeds in a layer-wise manner. Thus, as the number of layers increases, the referenced absolute error can propagate in a relevant way, crippling the ability of the algorithm to converge towards a discrete solution. On the other hand, the *softmax* operator fully addresses the referenced issues. Regarding overestimation, the new operator provides no overestimation, allowing a precise computation of the *smax* operator and a more effective convergence to a discrete solution. In fact, for the same level of P , the absolute error of the *smax* operator is reduced by a factor of 1.5 in unfavorable situations up to 2.4 in more favorable situations. In the scope of work, a P value of 40 was considered, being an effective compromise between precision and problem non-linearity. The value of P can be raised, but no relevant practical advantage was observed; however, the increase of the referenced constant increases the problem non-linearity, negatively affecting the numerical stability of the problem.

3.2.4. Algorithm Structure

The integration of the simplified fabrication model in the TO algorithm results in a procedure with numerous steps. Thus, a simplified flowchart of the optimization algorithm is shown in Algorithm 1.

Algorithm 1 Topology optimization algorithm structure with the fabrication model.

1. Build and save the neighborhood, N_e , for an efficient filtering operation;
 2. Build and save the support region, S_e , for an efficient application of the fabrication model;
 3. Initialize the design domain, \mathbf{x} ;
 4. Compute the physical densities, ρ , using Equations (7) and (8);
 5. Compute the print densities, ξ . In the layer-wise loop following print direction, apply Equations (13) and (14);
 6. Optimization loop:
 - (a) solve the structural problem ($\mathbf{K}(\xi)\mathbf{U} = \mathbf{F}$), using the element stiffness matrix given by Equation (3) or Equation (4), where ρ shall be replaced by ξ ;
 - (b) compute sensitivity $\partial f / \partial \xi$ based on print densities (Equation (17) or Equation (18));
 - (c) update sensitivities using the sensitivity information of the fabrication model. In a layer-wise loop following the reversed print direction, apply Equations (19) and (20) in order to update them;
 - (d) perform the filtering operation in order to obtain the final sensitivities using Equation (12).
 - (e) calculate new \mathbf{x} using an optimizer
 - (f) compute physical densities, ρ , using Equations (7) and (8);
 - (g) Compute print densities, ξ . In a layer-wise loop following the print direction, apply Equations (13) and (14)
 - (h) return to Sub-step (a) or break the loop if the solution has converged
-

3.3. Implementation

This implementation is aligned with the architecture proposed in [66]. The quality of the resultant solutions (ideally void (zero) and solid (one)) was evaluated using an indicator denominated as a measure of non-discreteness, M_{nd} . This indicator can be evaluated as [39]:

$$M_{nd} = \sum_{e=1}^n 4.0\xi_e(1.0 - \xi_e)/n, \tag{27}$$

where zero means that the design is fully discrete (there are no intermediate densities) and one means that the design is full of intermediates densities (for $V_f = 0.5$). The optimization problem was solved with the gradient-based Method of Moving Asymptotes (MMA) [67], using the default

parameters unless otherwise specified. The parameter η was set to three using SIMP and six using RAMP. Additionally, the parameter V_f was set to 0.5. Regarding Heaviside filtering, the filtering radius was set to four units; the parameter β was set to two and then doubled at Iterations 100, 150, 200, and 250; and finally, the parameter φ was set to 0.5. Regarding fabrication models, the parameters P , ρ_0 , and ϵ were set to 40, 0.5, and 1×10^{-4} , respectively, following Langelaar [50]. Unless otherwise specified, the build direction of fabrication was considered to be from bottom to top (upwards).

4. Examples

In order to increase manufacturability, in particular SLM, the initial designs resulting from the presented methodology always considered a minimum member size constraint imposed by TO filter. Unless otherwise stated, the filter radius was set to three elements in width. The overhang constraint may or may not be considered. If considered, the model is denominated as restricted. If not considered, the model is denominated as unrestricted.

4.1. Comparative Study

This section presents the topology optimization results of two well-known problems. The first problem, a cantilever structure, is depicted in Figure 3a, which is discretized by a regular quadrilateral mesh of 160×100 elements. The second problem, MBB, is depicted in Figure 3b, discretized by a regular quadrilateral mesh of 240×80 elements using symmetry conditions. Both problems consider unitary forces in the depicted direction.

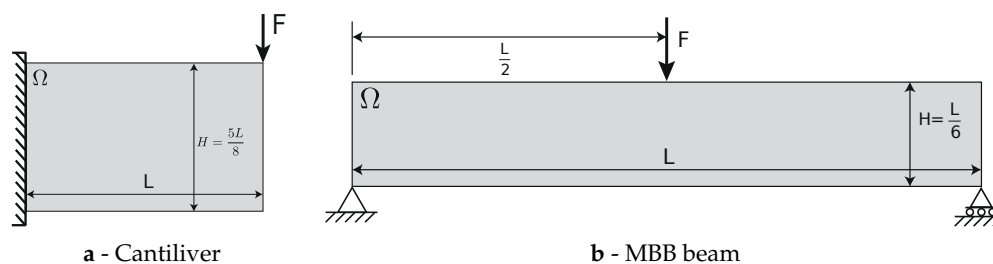


Figure 3. Benchmark problems' definition [55,68].

Figure 4 presents a compilation of the results of the cantilever problem at Iterations 20, 90, 150, and 300. Each subfigure contains two similar analyses, the difference being on the structural equilibrium evaluation. The simulation on the left used MSC Nastran code with a full integration rule to perform the structural equilibrium, while the analysis on the right used an approximated FE model presented in Andreassen et al. [66] and Sigmund [69]. Figure 5 presents a compilation of the results of the MBB problem at Iterations 20, 90, 150, and 300. Similar to the previous problem, each left subfigure used MSC Nastran to evaluate the structural equilibrium, while each right half used an approximated FE model presented in Andreassen et al. [66] and Sigmund [69].

Table 1 presents the final results at Iteration 300 of the cantilever and MBB problems, where it is possible to compare different variables such as FE model precision, the material interpolation models (SIMP or RAMP), and solution performance without (unrestricted) and with (restricted) the severe restriction of the simplified fabrication model.

After a close analysis of Figures 4 and 5, as well as Table 1, it becomes clear that the precision of the structural equilibrium had limited relevance even with such highly non-linear operators such as the fabrication model in a general perspective. However, Figure 4o is an exception, because a problematic member appeared (gray) with approximated structural equilibrium and not with MSC Nastran. Regarding filtering, the material interpolation model influenced the minimum member size solution. The RAMP model produced solutions with a larger minimum member size, but the final solutions were in accordance with the published results [66,69]. Moreover, the RAMP model allowed

material to grow out of the void, while SIMP did not. However, the numerical stability of SIMP combined with the topological “morphing” capabilities [56] makes the decision of the best material interpolation model somehow unclear. In the scope of this work, the SIMP model was used in the subsequent analysis since it is an industry standard.

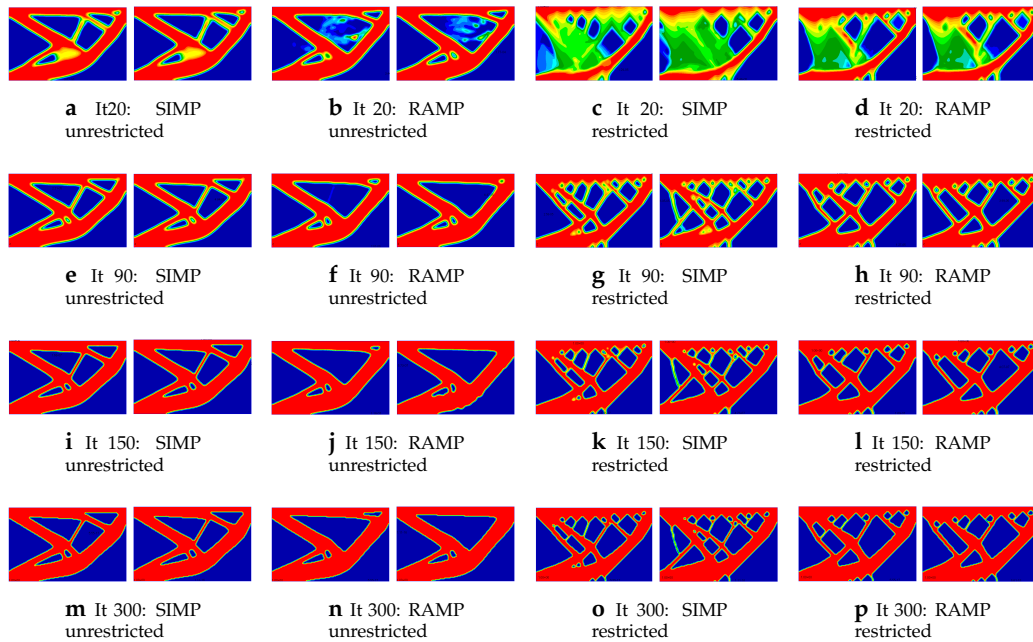


Figure 4. Topology optimization of the cantilever problem at Iterations 20, 90, 150, and 300. In each subfigure, the left image uses the full precision structural equilibrium, and the right image uses approximate structural equilibrium. SIMP, Solid Isotropic Material with Penalization; RAMP, Rational Approximation of Material Properties.

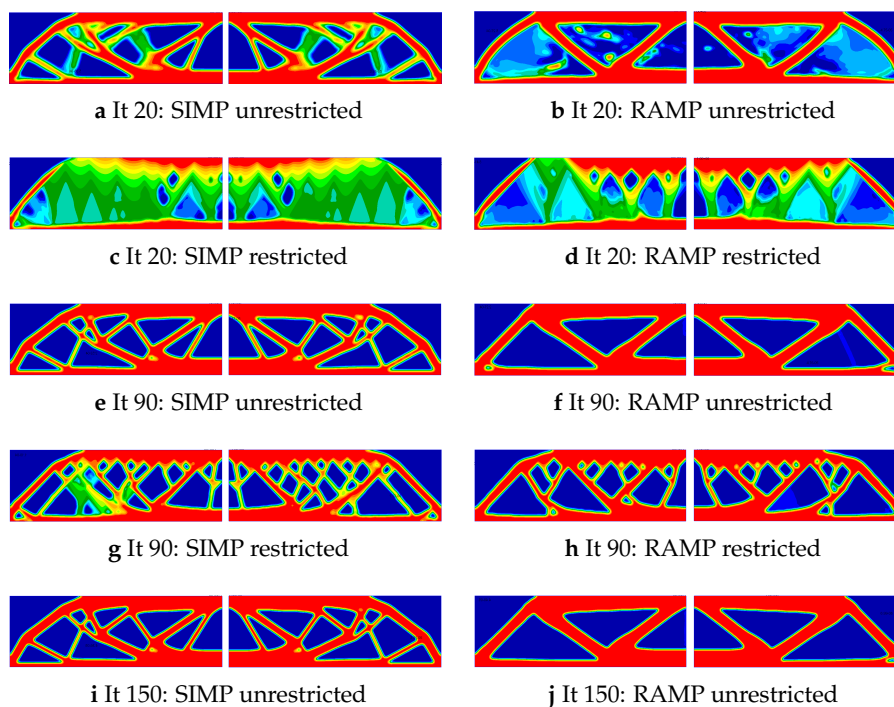


Figure 5. *Cont.*

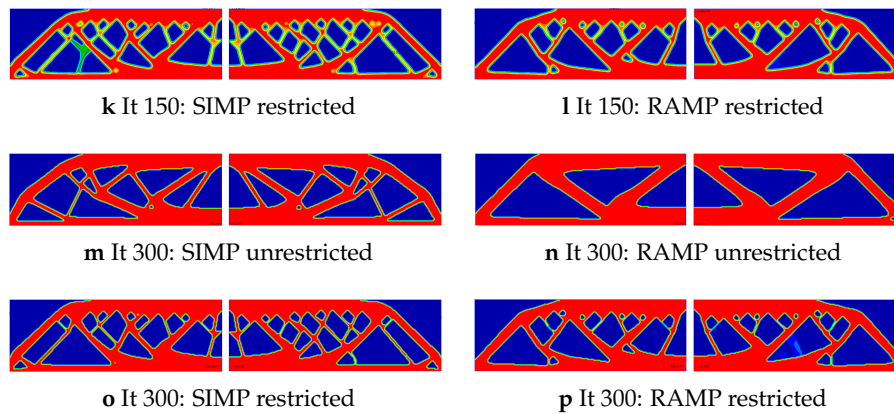


Figure 5. Topology optimization of the MBB problem at Iterations 20, 90, 150, and 300. In each subfigure, the left image uses full precision structural equilibrium, and the right image uses approximate structural equilibrium.

Table 1. Overview of the topology optimization of the cantilever and MBB problems at Iteration 300 in terms of Compliance (C) and the measure of non-discreteness level (M_{nd}).

	SIMP				RAMP			
	MSC Nastran		Aprox Model		MSC Nastran		Aprox Model	
	C	M_{nd} (%)						
Cantilever Problem								
Unrestricted	1.0	0.7	1.004	0.8	1.012	0.8	1.015	0.5
Restricted	1.058	0.6	1.051	1.0	1.066	0.8	1.038	0.1
MBB Problem								
Unrestricted	1.0	1.0	1.0	1.0	1.037	0.9	1.037	0.5
Restricted	1.049	0.4	1.049	0.7	1.054	1.0	1.055	1.4

Figure 6a,c shows the convergence curves of the cantilever and MBB problems using the original and modified (*softmax*) simplified fabrication models. The results consider the SIMP model and the approximated structural equilibrium. Moreover, a solution without the fabrication model is also included for reference purposes. The non-linearity of the referenced model with Heaviside filtering led to numerical instability in the initial iterations. At this point, the evaluation of the convergence properties resulting from the original and modified smooth max functions was required, and the initial instability made it less clear. Thus, this issue can be tackled by reducing the init parameter, s_0 (from [67]), to 0.05 [70], making the convergence slower in the initial iterations, but perfectly smooth. The overall convergence with original and modified smooth max functions remained similar, and an overview of the final iteration can be seen in Table 2. In these two problems, the modified version led to a marginal increase in compliance when compared to the original. On the other hand, Figure 6b,d depicts the evolution of the measure of non-discreteness M_{nd} . The modified filter showed a greater ability to converge to discrete solutions as depicted in Figure 7. This ability should be related to a more precise computation of the *smax* operator. The final values of M_{nd} are given in Table 2.

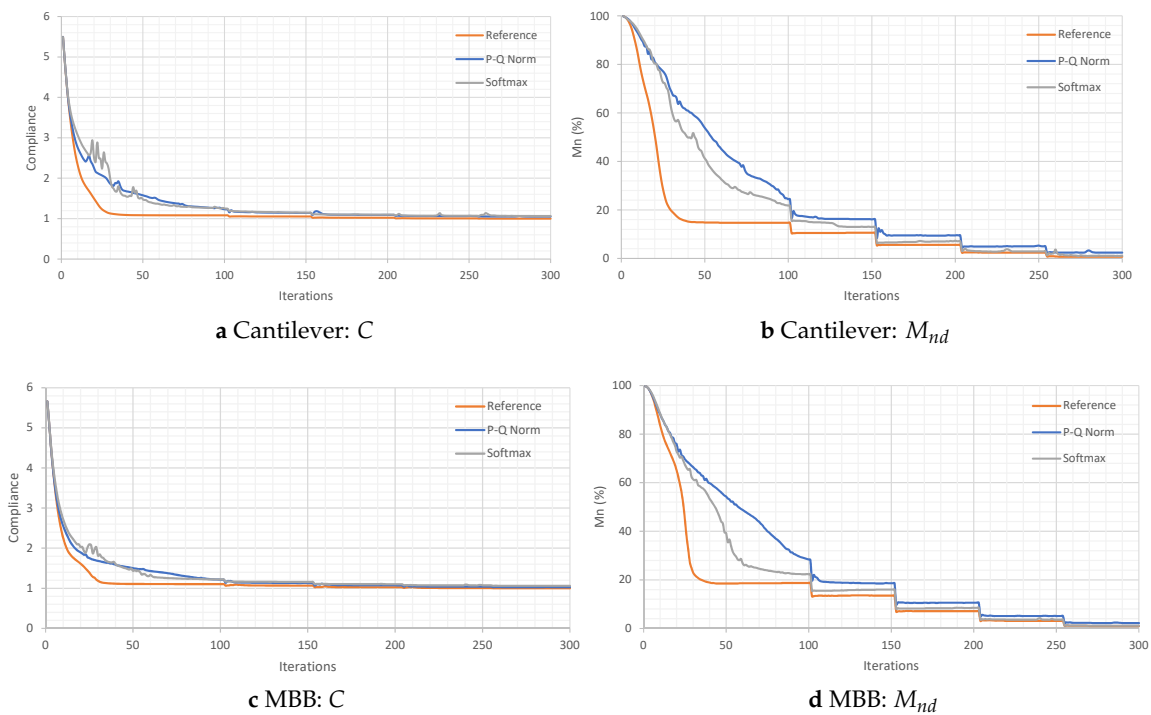


Figure 6. Comparison of the cantilever and MBB problems' topology optimization with the original and modified fabrication models.

Table 2. Overview of the cantilever and MBB problems' topology optimization with the original and modified fabrication models.

	Reference		P-Q Norm		Softmax	
	C	M_{nd}	C	M_{nd}	C	M_{nd}
Cantilever Problem	1.000	0.7	1.052	2.4	1.066	1.1
MBB Problem	1.000	1.0	1.028	2.2	1.061	1.1

The cantilever and MBB topology optimization problems presented in Figures 4 and 5 (SIMP restricted) are similar to the ones shown in Figure 7. The difference between them is the referenced change on the s_0 parameter of the MMA. Both simulations converged to self-supporting designs; however, different designs were observed, corresponding to different minima solutions.

In short, the proposed modified fabrication model addressed the issues identified by Langelaar [51] such as the performance of s_{max} , the high level of intermediate densities, and the problematic grey scale member. The proposed new s_{max} operator provided smaller error, no overestimation, and no additional parameter, and thus, the filter showed better ability to use fewer intermediate densities. For instance, on the cantilever and MBB problems at Iteration 100, the use of the new operator led to a reduction of the intermediate densities by 11% and 23%, respectively (consult Figure 6b,d). Regarding the problematic grey scale member, it should be related to the precision of structural equilibrium and not with fabrication model.

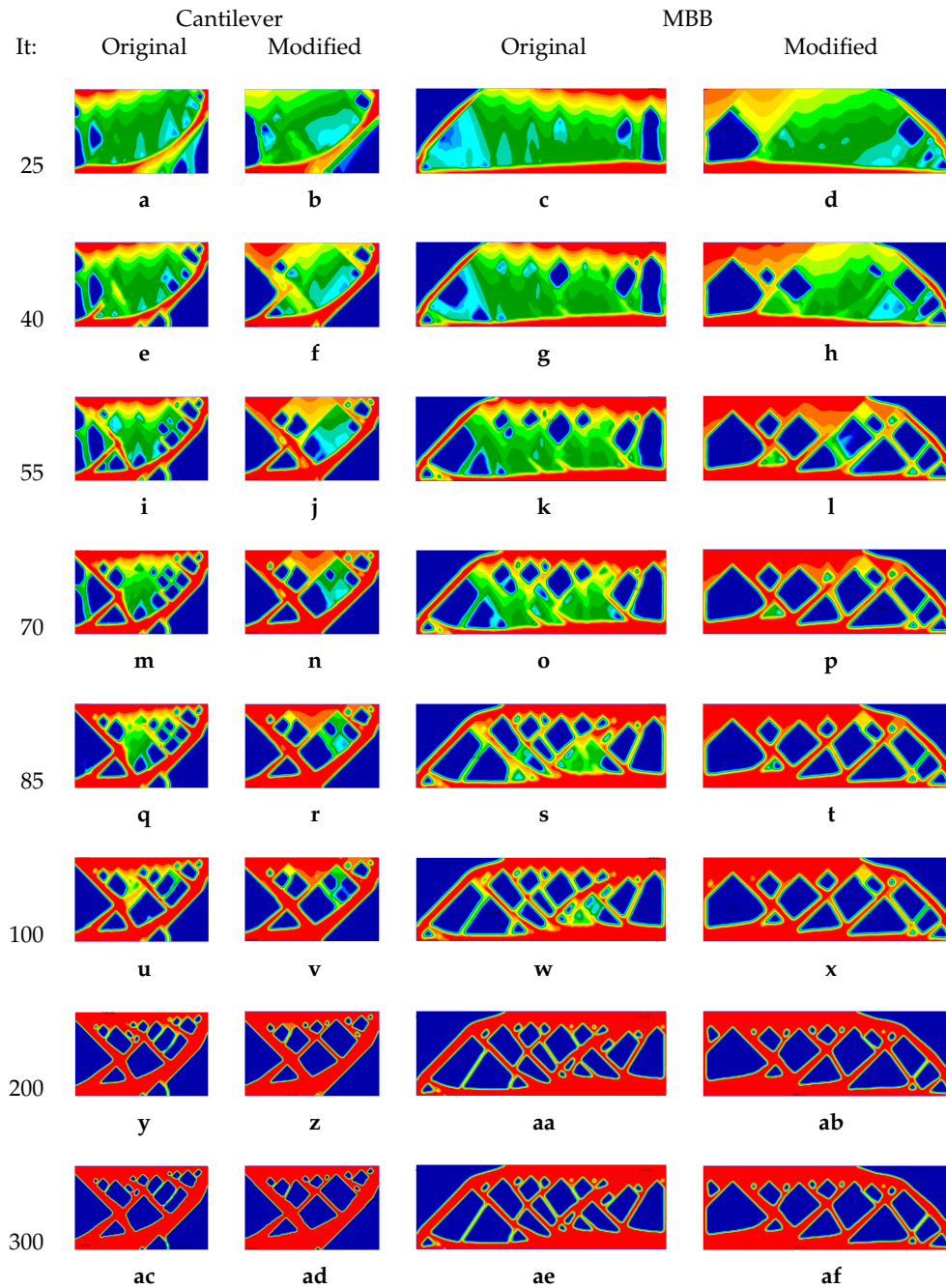


Figure 7. Comparison of the topology optimization problem of MBB using the original and modified version of the fabrication model.

5. A 3D Case Study

The section presents the TO results of the Sentinel-1 Antenna Support Bracket (approximated dimensions were used, since the real ones were not available). Figure 8 presents the available design domain, as well as boundary conditions. As depicted in the figure, the zero-displacement condition was applied to the four corners of the bracket, while the force was at its tip. The TO load case consisted of three subcases: (i) unitary force in the X direction, (ii) unitary force in the Y direction, and (iii) unitary force in the Z direction. Taking into consideration the maximum characteristic length of the part of 250 mm, a minimum member size constraint of 4.5 mm was considered (approximately a radius of three elements), as well as the overhang constraint. Moreover, a supporting region of five elements was used. Figures 9 and 10 present interactive models of the obtained material distribution

considering $V_f = 0.3$. In the design of Figure 9, the printing direction was aligned to the Z axis shown in Figure 8, and the faces of the design domain at Z were considered to be supported by support structures that connected the part to the base plate. The bottom oblique face (all the way to its tip) respected the overhang constraint; however, some support structures on its tip (at least) are recommended in order to avoid excessive thermo-mechanical warping. In the design of Figure 10, the printing direction was aligned to the X axis shown in Figure 8, and the faces of the design domain at X were considered to be supported by support structures that connected the part to the base plate. Some support structures on its tip (at least) are also recommended (for the same reasons) in order to avoid excessive thermo-mechanical warping.

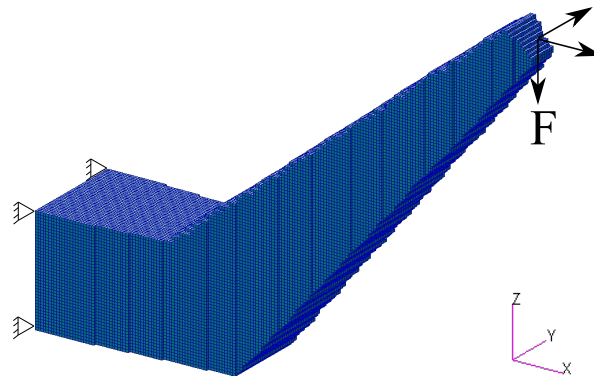


Figure 8. Topology Optimization (TO) design volume and boundary conditions.

The presented results showed that the algorithm was able to produce a self-supporting design in the 3D domain, as well. Moreover, the self-supporting design of Figure 9 had a similar compliance level when compared with the unrestricted solution. In fact, the restricted design suffered a marginal increase in compliance of 2%. On the other hand, the self-supporting design of Figure 10 led to an important increase in compliance (23%) when compared with the unrestricted solution.

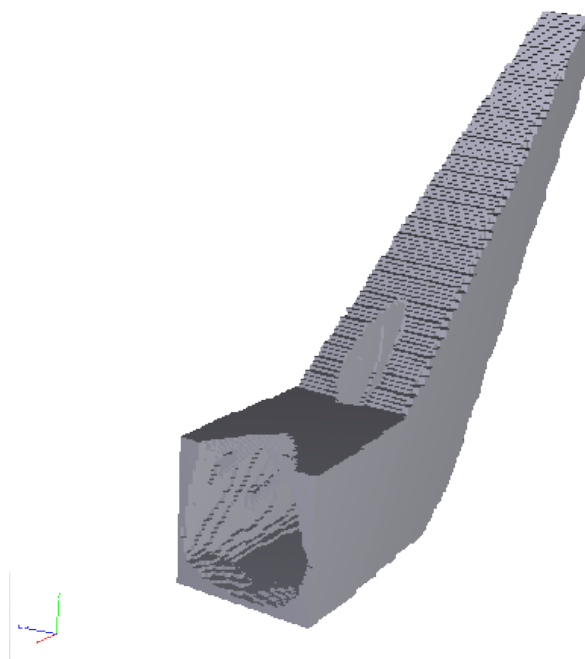


Figure 9. TO result considering the Z axis as the printing direction.

From a manufacturing and post-processing point of view, the major advantage of considering the overhang constraint was related to the reduction of support structures. In fact, the design can change significantly in order to become self-supporting and avoid the use of support structures. This advantage comes with a cost of compliance and computational time. On the other hand, internal support structures represent costs in terms of raw material, building time, and post-processing (i.e., cutting and machining). Moreover, their removal can pose a major challenge if they are internal to the design volume due to access and/or the risk of rupture of thin structural members during cutting and machining operations.

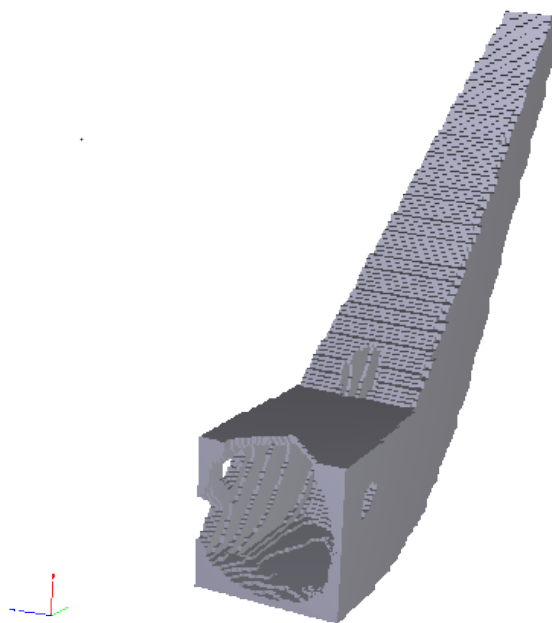


Figure 10. TO result considering the X axis as the printing direction.

6. Concluding Remarks

This study presented a computational methodology capable of providing initial solid designs for metal AM, and its performance was evaluated via a comparative study. The final methodology showed an improved capability of converging towards a discrete solution, having considerable relevance. In fact, a solution with a high level of intermediate densities has little practical use. However, the modified fabrication model was able to provide solutions with higher compliance when compared to the original. On the other hand, the compliance difference had limited relevance due to the small difference.

The initial self-supporting designs provided by the presented methodology allowed controlling the minimum member size and the overhang features in a closed computational environment, which was performance driven. Moreover, the resultant designs took advantage of the freedom provided by SLM, and TO played an important role in the search for optimal material distribution. Moreover, the referenced distribution can reduce the need for support structures.

Author Contributions: Conceptualization, B.B. and A.A.-C.; methodology, B.B. and A.A.-C.; software, B.B.; validation and formal analysis, B.B.; investigation, B.B.; writing, original draft preparation, B.B.; writing, review and editing, B.B., A.A.-C., and R.A.F.V.; project administration, A.A.-C.; funding acquisition, A.A.-C.

Funding: This research was funded by the Portuguese Foundation for Science and Technology (FCT) under the projects CENTRO-01-0145-FEDER-029713 by UE/FEDER through the programs CENTRO 2020 and COMPETE 2020 and UID/EMS/ 00481/2013-FCT under CENTRO-01-0145-FEDER-022083. Additional funding was provided by program CENTRO 2020 and UE/FEDER through the project CENTRO-01-0247-FEDER-024039, designated as

ADVANSS. Finally, the Portuguese Foundation for Science and Technology (FCT) provided additional funding via the scholarship SFRH/BD/120779/2016.

Acknowledgments: The authors gratefully acknowledge the financial support of the Portuguese Foundation for Science and Technology (FCT), program CENTRO 2020, and UE/FEDER. The authors also acknowledge the help of Krister Svanberg for providing MATLAB code, which was important for a successful Python implementation, and Matthijs Langelaar for providing article clarifications.

Conflicts of Interest: The authors declare no conflict of interest.

References

- Murr, L.E.; Gaytan, S.M.; Ramirez, D.A.; Martinez, E.; Hernandez, J.; Amato, K.N.; Shindo, P.W.; Medina, F.R.; Wicker, R.B. Metal Fabrication by Additive Manufacturing Using Laser and Electron Beam Melting Technologies. *J. Mater. Sci. Technol.* **2012**, *28*, 1–14. [[CrossRef](#)]
- Aremu A.; Ashcroft I.; Hague R.; Wildman R.; Tuck C. *Suitability of SIMP and BESO Topology Optimization Algorithms for Additive Manufacture*; Wolfson School of Mechanical and Manufacturing Engineering: Loughborough, UK, 2010.
- Clausen, A. Topology Optimization for Additive Manufacturing. Ph.D. Thesis, DTU Mechanical Engineering, Technical University of Denmark, Kongens Lyngby, Denmark, 2016.
- Komi, E. *Topology Optimized in Design for Additive Manufacturing*; AM-Teknologista uutta Liiketoimintaa, Report of VTT Technical Research Centre; VTT: Helsinki, Finland, 2014.
- Matt, D.T.; Rauch, E.; Dallasega, P. Trends towards Distributed Manufacturing Systems and Modern Forms for their Design. *Procedia CIRP* **2015**, *33*, 185–190. [[CrossRef](#)]
- Attaran, M. Additive manufacturing: The most promising technology to alter the supply chain and logistics. *J. Serv. Sci. Manag.* **2017**, *10*, 189–206. [[CrossRef](#)]
- Attaran, M. The rise of 3-D printing: The advantages of additive manufacturing over traditional manufacturing. *Bus. Horiz.* **2017**, *60*, 677–688. [[CrossRef](#)]
- Fera, M.; Fruggiero, F.; Lambiase, A.; Macchiaroli, R. State of the art of additive manufacturing: Review for tolerances, mechanical resistance and production costs. *Cogent Eng.* **2016**, *3*, 1261503. [[CrossRef](#)]
- Rosen, D.W. Computer-Aided Design for Additive Manufacturing of Cellular Structures. *Comput.-Aided Des. Appl.* **2007**, *4*, 585–594. [[CrossRef](#)]
- Weller, C.; Kleer, R.; Piller, F.T. Economic implications of 3D printing: Market structure models in light of additive manufacturing revisited. *Int. J. Prod. Econ.* **2015**, *164*, 43–56. [[CrossRef](#)]
- Anstaett, C.; Schafnitzel, M.; Seidel, C.; Reinhart, G. Laser-based Powder Bed Fusion of 3D-Multi-Material-Parts of Copper-Chrome-Zirconia and Tool Steel. In Proceedings of the European Powder Metallurgy Association Proceedings, Milan, Italy, 1–5 October 2017.
- Bobbio, L.D.; Otis, R.A.; Borgonia, J.P.; Dillon, R.P.; Shapiro, A.A.; Liu, Z.K.; Beese, A.M. Additive manufacturing of a functionally graded material from Ti-6Al-4V to Invar: Experimental characterization and thermodynamic calculations. *Acta Mater.* **2017**, *127*, 133–142. [[CrossRef](#)]
- Kotoban, D.; Aramov, A.; Tarasova, T. Possibility of Multi-material Laser Cladding Fabrication of Nickel Alloy and Stainless Steel. *Phys. Procedia* **2016**, *83*, 634–646. [[CrossRef](#)]
- DebRoy, T.; Wei, H.L.; Zuback, J.S.; Mukherjee, T.; Elmer, J.W.; Milewski, J.O.; Beese, A.M.; Wilson-Heid, A.; De, A.; Zhang, W. Additive manufacturing of metallic components—Process, structure and properties. *Prog. Mater. Sci.* **2018**, *92*, 112–224. [[CrossRef](#)]
- Balla, V.K.; Xue, W.; Bose, S.; Bandyopadhyay, A. Laser-assisted Zr/ZrO₂ coating on Ti for load-bearing implants. *Acta Biomater.* **2009**, *5*, 2800–2809. [[CrossRef](#)] [[PubMed](#)]
- Zhang, Y.; Sahasrabudhe, H.; Bandyopadhyay, A. Additive manufacturing of Ti-Si-N ceramic coatings on titanium. *Appl. Surf. Sci.* **2015**, *346*, 428–437. [[CrossRef](#)]
- Fang, Z.; Lu, L.; Chen, L.; Guan, Y. Laser Polishing of Additive Manufactured Superalloy. *Procedia CIRP* **2018**, *71*, 150–154.
- Ai, L.; Gao, X.L. Metamaterials with negative Poisson's ratio and non-positive thermal expansion. *Compos. Struct.* **2017**, *162*, 70–84. [[CrossRef](#)]
- Wei, K.; Peng, Y.; Wang, K.; Duan, S.; Yang, X.; Wen, W. Three dimensional lightweight lattice structures with large positive, zero and negative thermal expansion. *Compos. Struct.* **2018**, *188*, 287–296. [[CrossRef](#)]

20. Holmström, J.; Partanen, J.; Tuomi, J.; Walter, M. Rapid manufacturing in the spare parts supply chain: Alternative approaches to capacity deployment. *J. Manuf. Technol. Manag.* **2010**, *21*, 687–697. [[CrossRef](#)]
21. Nickels, L. AM and aerospace: An ideal combination. *Met. Powder Rep.* **2015**, *70*, 300–303. [[CrossRef](#)]
22. Kelly, S.M. *Volume 1: Development and Measurement Analysis of Design Data for Laser Powder Bed Fusion Additive Manufacturing of Nickel Alloy 625*; Technical Report; EWI: Columbus, OH, USA, 2014.
23. Huang, Y.; Leu, M.C.; Arbor, A. Additive Manufacturing: Current State, Future Potential, Gaps and Needs, and Recommendations. *ASME J. Manuf. Sci. Eng.* **2015**, *137*, 1087–1357. [[CrossRef](#)]
24. Thompson, M.K.; Moroni, G.; Vaneker, T.; Fadel, G.; Campbell, R.I.; Gibson, I.; Bernard, A.; Schulz, J.; Graf, P.; Ahuja, B.; et al. Manufacturing Technology Design for Additive Manufacturing: Trends, opportunities, considerations and constraints. *CIRP Ann.* **2016**, *65*, 737–760. [[CrossRef](#)]
25. Thomas, D. The Development of Design Rules for Selective Laser Melting the Development of Design Rules for Selective Laser Melting. Ph.D. Thesis, University of Wales Institute, Cardiff, UK, 2009.
26. Vayre, B.; Vignat, F.; Villeneuve, F. Designing for Additive Manufacturing. *Procedia CIRP* **2012**, *3*, 632–637. [[CrossRef](#)]
27. Vayre, B.; Vignat, F.; Villeneuve, F. Identification on some design key parameters for additive manufacturing: Application on Electron Beam Melting. *Procedia CIRP* **2013**, *7*, 264–269. [[CrossRef](#)]
28. Adam, G.A.O.; Zimmer, D. CIRP Journal of Manufacturing Science and Technology Design for Additive Manufacturing—Element transitions and aggregated structures. *CIRP J. Manuf. Sci. Technol.* **2014**, *7*, 20–28. [[CrossRef](#)]
29. Klahn, C.; Leutenecker, B.; Meboldt, M. Design Strategies for the Process of Additive Manufacturing. *Procedia CIRP* **2015**, *36*, 230–235. [[CrossRef](#)]
30. Kranz, J.; Herzog, D.; Emmelmann, C.; Kranz, J.; Herzog, D. Design guidelines for laser additive manufacturing of lightweight structures in TiAl6V4. *J. Laser Appl.* **2016**, *27*, S14001. [[CrossRef](#)]
31. Lemu, H.G.; Gebisa, A.W. Design for manufacturing to design for Additive Manufacturing: Analysis of implications for design optimality and product sustainability. *Procedia Manuf.* **2017**, *13*, 724–731.
32. Sossou, G.; Demoly, F.; Montavon, G.; Gomes, S. Journal of Computational Design and Engineering An additive manufacturing oriented design approach to mechanical assemblies. *J. Comput. Des. Eng.* **2018**, *5*, 3–18.
33. Joshi, S.C.; Sheikh, A.A. 3D printing in aerospace and its long-term sustainability. *Virtual Phys. Prototyp.* **2015**, *10*, 175–185. [[CrossRef](#)]
34. Reddy K., S.N.; Ferguson, I.; Frecker, M.; Simpson, T.W.; Dickman, C.J. Topology Optimization Software for Additive Manufacturing: A Review of Current Capabilities and a Real-World Example. In Proceedings of the ASME 2016 International Design Engineering Technical Conferences and Computers and Information in Engineering Conference, Charlotte, NC, USA, 21–24 August 2016.
35. Mirzendehtdel, A.M.; Suresh, K. Support structure constrained topology optimization for additive manufacturing. *Comput.-Aided Des.* **2016**, *81*, 1–13. [[CrossRef](#)]
36. Walton, D.; Moztarzadeh, H. Design and Development of an Additive Manufactured Component by Topology Optimisation. *Procedia CIRP* **2017**, *60*, 205–210. [[CrossRef](#)]
37. Allaire, G.; Dapogny, C.; Estevez, R.; Faure, A.; Michailidis, G. Structural optimization under overhang constraints imposed by additive manufacturing technologies. *J. Comput. Phys.* **2017**, *351*, 295–328. [[CrossRef](#)]
38. Guo, X.; Zhou, J.; Zhang, W.; Du, Z.; Liu, C.; Liu, Y. Self-supporting structure design in additive manufacturing through explicit topology optimization. *Comput. Methods Appl. Mech. Eng.* **2017**, *323*, 27–63. [[CrossRef](#)]
39. Sigmund, O. Morphology-based black and white filters for topology optimization. *Struct. Multidiscip. Optim.* **2007**, *33*, 401–424. [[CrossRef](#)]
40. Svanberg, K.; Svärd, H. Density filters for topology optimization based on the Pythagorean means. *Struct. Multidiscip. Optim.* **2013**, *48*, 859–875. [[CrossRef](#)]
41. Leary, M.; Merli, L.; Torti, F.; Mazur, M.; Brandt, M. Optimal topology for additive manufacture: A method for enabling additive manufacture of support-free optimal structures. *Mater. Des.* **2014**, *63*, 678–690. [[CrossRef](#)]
42. Mass, Y.; Amir, O. Topology optimization for additive manufacturing: Accounting for overhang limitations using a virtual skeleton. *Addit. Manuf.* **2017**, *18*, 58–73. [[CrossRef](#)]

43. Liu, C.; Du, Z.; Zhang, W.; Zhu, Y.; Guo, X. Additive Manufacturing-Oriented Design of Graded Lattice Structures Through Explicit Topology Optimization. *J. Appl. Mech.* **2017**, *84*, 081008-81020. [[CrossRef](#)]
44. Brackett, D.; Ashcroft, I.; Hague, R. *Topology Optimization for Additive Manufacturing*; Wolfson School of Mechanical and Manufacturing Engineering, Loughborough University: Loughborough, UK, 2011.
45. Maskery, I.; Aboulkhair, N.; Aremu, A.; Tuck, C.; Ashcroft, I.; Wildman, R.; Hague, R. A mechanical property evaluation of graded density Al-Si10-Mg lattice structures manufactured by selective laser melting. *Mater. Sci. Eng. A* **2016**, *670*, 264–274. [[CrossRef](#)]
46. Zhao, D.; Li, M.; Liu, Y. Self-supporting Topology Optimization for Additive Manufacturing. *arXiv* **2017**, arXiv:1708.07364.
47. Qian, X. Undercut and overhang angle control in topology optimization: A density gradient based integral approach. *Int. J. Numer. Methods Eng.* **2016**, *111*, 247–272. [[CrossRef](#)]
48. Garaigordobil, A.; Ansola, R. A new overhang constraint for topology optimization of self-supporting structures in additive manufacturing. *Struct. Multidiscip. Optim.* **2018**, *58*, 2003–2017. [[CrossRef](#)]
49. Mezzadri, F.; Bouriakov, V.; Qian, X. Topology optimization of self-supporting support structures for additive manufacturing. *Addit. Manuf.* **2018**, *21*, 666–682. [[CrossRef](#)]
50. Langelaar, M. An additive manufacturing filter for topology optimization of print-ready designs. *Struct. Multidiscip. Optim.* **2017**, *55*, 871–883. [[CrossRef](#)]
51. Langelaar, M. Topology optimization of 3D self-supporting structures for additive manufacturing. *Addit. Manuf.* **2016**, *12*, 60–70. [[CrossRef](#)]
52. Hoffarth, M.; Gerzen, N.; Pedersen, C. ALM Overhang Constraint in Topology Optimization for Industrial Applications. In Proceedings of the 12th World Congress on Structural and Multidisciplinary Optimisation, Braunschweig, Germany, 5–9 June 2017.
53. Gaynor, A.T.; Meisel, N.A.; Williams, C.B.; Guest, J.K. Topology Optimization for Additive Manufacturing: Considering Maximum Overhang Constraint. In Proceedings of the 15th AIAA/ISSMO Multidisciplinary Analysis and Optimization Conference, Atlanta, GA, USA, 16–20 June 2014.
54. Gaynor, A.T. Topology Optimization Algorithms for Additive Manufacturing. Ph.D. Thesis, The Johns Hopkins University, Baltimore, MD, USA, 2015.
55. Gaynor, A.T.; Guest, J.K. Topology optimization considering overhang constraints: Eliminating sacrificial support material in additive manufacturing through design. *Struct. Multidiscip. Optim.* **2016**, *54*, 1157–1172. [[CrossRef](#)]
56. Johnson, T.E.; Gaynor, A.T. Three-dimensional projection-based topology optimization for prescribed-angle self-supporting additively manufactured structures. *Addit. Manuf.* **2018**, *24*, 667–686. [[CrossRef](#)]
57. Rozvany, G.I.N.; Lewiński, T. *Topology Optimization in Structural and Continuum Mechanics*; Springer: Vienna, Italy, 2014.
58. Deaton, J.D.; Grandhi, R.V.; Deaton, J.D.; Grandhi, R.V. A survey of structural and multidisciplinary continuum topology optimization: Post 2000. *Struct. Multidiscip. Optim.* **2014**, *49*, 1–38. [[CrossRef](#)]
59. Bendsoe, M.P. Optimal shape design as a material distribution problem. *Struct. Optim.* **1989**, *1*, 193–202. [[CrossRef](#)]
60. Bendsoe, M.P.; Sigmund, O.O. *Topology Optimization: Theory, Methods, and Applications*; Springer: Berlin/Heidelberg, Germany, 2004.
61. Stolpe, M.; Svanberg, K. An Interpolation Model for Minimum Compliance Topology Optimization. *Struct. Multidiscip. Optim.* **2001**, *22*, 116–124. [[CrossRef](#)]
62. Bruns, T.E.; Tortorelli, D.A. Topology optimization of non-linear elastic structures and compliant mechanisms. *Comput. Methods Appl. Mech. Eng.* **2001**, *190*, 3443–3459. [[CrossRef](#)]
63. Bourdin, B. Filters in topology optimization. *Int. J. Numer. Methods Eng.* **2001**, *50*, 2143–2158. [[CrossRef](#)]
64. Wang, F.; Lazarov, B.S.; Sigmund, O. On projection methods, convergence and robust formulations in topology optimization. *Struct. Multidiscip. Optim.* **2011**, *43*, 767–784. [[CrossRef](#)]
65. Lange, M.; Zuhke, D.; Holz, O.; Villmann, T. Applications of lp-Norms and their Smooth Approximations for Gradient Based Learning Vector Quantization. In Proceedings of the ESANN 2014 Proceedings, European Symposium on Artificial Neural Networks, Computational Intelligence and Machine Learning, Bruges, Belgium, 23–25 April 2014.
66. Andreassen, E.; Clausen, A.; Schevenels, M.; Lazarov, B.S.; Sigmund, O. Efficient topology optimization in MATLAB using 88 lines of code. *Struct. Multidiscip. Optim.* **2011**, *43*, 1–16. [[CrossRef](#)]

67. Svanberg, K. The method of moving asymptotes—a new method for structural optimization. *Int. J. Numer. Methods Eng.* **1987**, *24*, 359–373. [[CrossRef](#)]
68. Rozvany, G.I.N. Exact analytical solutions for some popular benchmark problems in topology optimization. *Struct. Optim.* **1998**, *15*, 42–48. [[CrossRef](#)]
69. Sigmund, O. A 99 line topology optimization code written in Matlab. *Struct. Multidiscip. Optim.* **2001**, *21*, 120–127. [[CrossRef](#)]
70. Guest, J.K.; Asadpoure, A.; Ha, S.H. Eliminating beta-continuation from Heaviside projection and density filter algorithms. *Struct. Multidiscip. Optim.* **2011**, *44*, 443–453. [[CrossRef](#)]



© 2019 by the authors. Licensee MDPI, Basel, Switzerland. This article is an open access article distributed under the terms and conditions of the Creative Commons Attribution (CC BY) license (<http://creativecommons.org/licenses/by/4.0/>).